Neuromorphic nanoelectronic materials

Article *in* Nature Nanotechnology · March 2020

DOI: 10.1038/s41565-020-0647-z

2 authors, including:

Vinod Kumar Sangwan
Northwestern University
145 PUBLICATIONS **6,627** CITATIONS

SEE PROFILE

nature nanotechnology

FOCUS | REVIEW ARTICLE

https://doi.org/10.1038/s41565-020-0647-z

Neuromorphic nanoelectronic materials

Vinod K. Sangwan[1] and Mark C. Hersam[1,2,3] ✉

Memristive and nanoionic devices have recently emerged as leading candidates for neuromorphic computing architectures. While top-down fabrication based on conventional bulk materials has enabled many early neuromorphic devices and circuits, bottom-up approaches based on low-dimensional nanomaterials have shown novel device functionality that often better mimics a biological neuron. In addition, the chemical, structural and compositional tunability of low-dimensional nanomaterials coupled with the permutational flexibility enabled by van der Waals heterostructures offers significant opportunities for artificial neural networks. In this Review, we present a critical survey of emerging neuromorphic devices and architectures enabled by quantum dots, metal nanoparticles, polymers, nanotubes, nanowires, two-dimensional layered materials and van der Waals heterojunctions with a particular emphasis on bio-inspired device responses that are uniquely enabled by low-dimensional topology, quantum confinement and interfaces. We also provide a forward-looking perspective on the opportunities and challenges of neuromorphic nanoelectronic materials in comparison with more mature technologies based on traditional bulk electronic materials.

Over the past two decades, significant advances have been achieved in artificial neural networks (ANNs) as a result of increased computational power, availability of big data and breakthroughs in training methods[1,2]. The resulting deep learning in ANNs is poised to impact diverse sectors including healthcare, security, robotics, Internet of Things and environmental sciences[2]. While ANNs enable more energy efficient algorithms than traditional approaches, they are typically realized using conventional von Neumann computing architectures where the transfer of data between physically separate logic and memory blocks results in processing bottlenecks and unwanted power consumption[1]. Inspired by the co-location of logic and memory, robustness against local failures, hyper-connectivity and parallel processing in the human brain, alternative neuromorphic computing architectures promise substantially lower power consumption by physically emulating neurons and synapses at the small circuit or device level[3–7]. Early successes in neuromorphic computing have relied heavily on conventional electronic materials, particularly silicon-based complementary metal–oxide–semiconductor (CMOS) spiking neural networks[3,4,8–10]. Prominent examples include the TrueNorth chip from IBM that can recognize disparate objects from video feeds in real-time[11] and the SpiNNaker Project within the European Union Human Brain Program that can execute cognitive tasks[12].

Since CMOS chips suffer from energy inefficient synaptic operations based on volatile random access memory (RAM), significant effort has been devoted to non-volatile memory (NVM) as a foundation for neuromorphic computing. Several NVM technologies have emerged such as phase-change memory[13], resistive random access memory (ReRAM)[14–17] and spin-torque transfer random access memory[18] that can simultaneously provide memory (that is, a weight storage unit) and logic units (that is, a dot-product machine)[10,19–21]. Among these NVMs, ReRAM cells or memristors have the advantage of smaller footprints and lower power consumption without compromising other metrics[8,9,16]. Memristive crossbar arrays have already demonstrated diverse functionality such as unsupervised pattern classification, multilayer perceptron networks and efficient solutions of differential equations[22–26]. The coexistence of NVM and multi-state switching in memristors also makes hybrid CMOS-memristive circuits promising for edge computing and Internet of Things, where local processing of analogue and digital data in mobile devices relaxes the need to access the cloud[8,27].

Conventional memristors based on bulk materials (for example, transition metal oxides) rely on top-down lithographic patterning that has limited control and tunability over neuromorphic functionality due to the strong dependence of the device response on the atomic-scale structure of defects. In contrast, emerging low-dimensional nanomaterials present unprecedented control over stoichiometry, defect engineering and interfacial chemistry, which underlie synaptic behaviour. Low-dimensional nanomaterials also possess quantum phase transitions, new state variables, electrostatic tunability and atomic-level control for reconfigurable switches and neuromorphic functions[28–32]. Within this class of materials, two-dimensional (2D) nanomaterials provide an open architecture for multiple electrodes, in situ probing, and spatiotemporal responses,[30,33–35] while zero-dimensional (0D) and one-dimensional (1D) nanomaterials enable highly sensitive covalent functionalization and redox chemistry for multi-bit states[36–39]. Promising results are also emerging from hybrid systems that integrate nanomaterials of different dimensionalities[31,40,41]. Due to their mechanical flexibility, low-dimensional nanomaterials are also facilitating the development of wearable neuromorphic applications such as afferent nerves and smart prosthetics[4,42]. Here, we review recent progress in the emerging field of neuromorphic nanoelectronic materials with a focus on how the properties of 0D, 1D and 2D nanomaterials and their van der Waals heterostructures enable unique neuromorphic responses compared to inorganic[8,14,15,18] and organic materials[36,37] whose neuromorphic potential has already been discussed extensively elsewhere[10,20,21,43].

Artificial synapses, neurons and networks

Neuromorphic computing hardware requires physical models at three different levels: (1) individual components such as artificial synapses and neurons; (2) networks of these neurons and synapses; (3) learning rules and training methods[4,8]. Historically, early attempts at understanding the mammalian brain focused on the physical aspects of neurons including the McCulloch–Pitts neuron[44] and Rosenblatt perceptron[45], which became the foundation for later improvements[46,47]. Briefly, the cell body of a neuron collects

[1]Department of Materials Science and Engineering, Northwestern University, Evanston, IL, USA. [2]Department of Chemistry, Northwestern University, Evanston, IL, USA. [3]Department of Electrical and Computer Engineering, Northwestern University, Evanston, IL, USA. ✉e-mail: m-hersam@northwestern.edu

and sums the charges provided through synaptic connections in the dendrites until the total charge reaches a threshold after which the neuron fires a spike along the axon[5]. The resulting spike is passed to other neurons connected via synapses that can either reinforce or inhibit the signal depending on synaptic weights. A more physiologically accurate Hodgkin–Huxley model[48] involves coupled differential equations with greater than 20 parameters such as the concentrations of K^+ and Na^+ ions, which became the basis for subsequent approximations[49,50]. Later research in neuroscience shifted the focus to the higher-level conceptual basis of learning, cognition and behaviour of populations of neurons, with the resulting models becoming the foundation for ANN architectures (for example, Hopfield networks) and learning rules (for example, Hebbian learning)[1,46,51].

Although hardware implementations began even before the invention of CMOS (for example, vacuum-tube hardware models)[52], implementation of software ANNs on CMOS hardware quickly took over due to consistent energy gains from integrated circuit miniaturization. The recent interest in revisiting hardware implementations has arisen from the imminent incapability of existing systems to handle exponentially growing computational and memory demands. For example, if data storage and communication continue to increase at the current rate, the total energy consumed by binary operations using CMOS will surpass ~10^{27} Joules in 2040, which exceeds the total energy being produced globally[9]. Therefore, lower energy CMOS alternatives are being explored based on non-von-Neumann computing architectures.

The simplest integrate-and-fire neuron can be made from a leaky capacitor that sums the current from the synapses with the leakage current helping to bring the neuron to a resting state. Since capacitors consume large areas in chips, more efficient neuron models use transistor circuits including Schmitt triggers, summing amplifiers and comparators to achieve spiking behaviour. A synapse is a simpler component involving two units—namely, a weight storage unit and an induction protocol unit that modifies the weight depending on spiking conditions. The earliest demonstration of a transistor as a synapse (that is, synaptic transistor) used a floating gate where hot electron injection and tunnelling stored or dissipated the charge on the floating gate, respectively, resulting in modulation of threshold voltage and conductivity (that is, synaptic weight) of the transistor (Fig. 1a,c(i))[53]. Similarly, gate bias hysteresis originating from charge traps in gate dielectrics also produces a learning device (Fig. 1c(ii)). Key advantages of synaptic transistors include the robustness of the design and the open channel that allows for multiple gate terminals to achieve spatiotemporal responses[54,55]. However, the lateral geometry of synaptic transistors implies a relatively large footprint, which is suboptimal for synapses where high density is critical[56].

An alternative synaptic device is a vertical memristor, which possesses a smaller size[16,57], enables 3D stacked memory[58] and combines both an induction protocol and memory into one device[9]. Bulk materials and switching mechanisms for conventional memristors have been reviewed extensively elsewhere[10,14,50,59,60]. In short, resistive switching in memristors can result from the formation and breakage of a metallic filament or modulation of a Schottky barrier via migration of defects or ionic species (Fig. 1b). Related phase-change memory devices display a metal-to-insulator transition due to local heating and rapid quenching (Fig. 1b)[13]. Memristive systems define current–voltage relations through coupled differential equations involving an internal state variable such as the spatial extension of dopant density[50]. Memristors can undergo either non-volatile resistive switching with different resistance states at zero bias (Fig. 1c(iii))[61], or volatile switching with a memristive loop at high biases and identical resistance states at zero bias (Fig. 1c(iv))[62]. In bipolar resistive switching, a reverse bias is required to switch the device ON and OFF, whereas both switching events can occur at the same bias polarity in unipolar switching[61,63]. In addition, two bipolar switches can be connected back-to-back to obtain complementary resistive switching (Fig. 1c(v))[64]. Recently, Mott memristors with multiple state variables have been explored for neuronal function such as Pearson–Anson neuristors[65]. Memcapacitor-based neurotransistors and diffusive memristors are additional candidates for leaky integrate-and-fire neurons[66,67].

Integration of artificial synapses and neurons into ANNs has been realized in many architectures including deep neural networks, spiking neural networks (SNNs), recurrent neural networks, and convolutional neural networks[4,8]. Hybrid CMOS-memristor chips have also achieved both supervised and unsupervised learning with on-chip and off-chip training methods[3,4,8]. Almost all of these circuits employ crossbar arrays where a practical challenge is to address individual synapse nodes. Several solutions exist including the one-transistor-one-memristor (1T1M) geometry, where the transistor acts as a selector to minimize sneak currents. Memristors alone can also enable selective addressing using two memristors in parallel or five memristors in a Wheatstone bridge that not only provide a selector but also allow positive, negative and zero weights for synapses[8]. Complexity in memristive systems at the device level can often imply simplicity at the circuit level[50,68–71]. For example, heterosynaptic plasticity involves a third modulatory terminal for additional control over simple Hebbian rules (that is, neurons that fire together wire together)[40,72–74]. Furthermore, a memtransistor possesses two memristive elements near the contacts of a Schottky transistor and a pinched hysteresis loop that can be further tuned by the gate terminal (Fig. 1c(vi))[33,74–77]. In this manner, a memtransistor not only integrates the 1T1M architecture within one device but also achieves bio-realistic hyper-connectivity and gate-tunable spike-timing-dependent plasticity (STDP)[33,78,79]. In the sections that follow, the unique properties of emerging nanomaterials will be explored as alternatives to these more conventional approaches to neuromorphic hardware[32].

Zero-dimensional neuromorphic nanomaterials

The optical properties of 0D nanomaterials are well-suited for neuromorphic implementation in photonic systems. Photonic devices enable parallel communication and hyper-connectivity since photon propagation does not have the same spatial and power density constraints as wires in electronic circuits. However, progress in this direction has been impeded by two issues. First, while linear media are preferred for optical communication, non-linear media are also needed to achieve signal gain[46]. Second, it has been challenging to develop effective memory components using purely optical signals. Therefore, hybrid optoelectronic systems are often employed where memory is realized in electronics and communication in photonics[80]. In the context of neural networks, 3D-printed diffraction gratings have been developed to classify 10,000 objects with an accuracy exceeding 80%[81]. On the other hand, 0D semiconducting quantum dots (QD) exhibit well-defined energy levels for optical processing, and 0D metal nanoparticles show size-tunable plasmonic responses that enable local gain (Fig. 2). In this manner, mode-locked lasers from InAs/InGaAs QDs have emulated both excitatory and inhibitory synaptic responses[82]. Here, the operating principle is enabled by the multi-band emission of QDs, although integration of colloidal QDs with photonic waveguides remains a challenge. Nevertheless, electro-photo-sensitive memristors have been realized using site-controlled quantum dots on GaAs/AlGaAs wafers where the conductance is tuned by either electrical or optical pulses[83,84].

Bottom-up QD synthesis results in atomically precise size, structure and chemical composition, providing highly tuned physical responses. For example, $CsPbBr_3$ perovskite colloidal QDs coupled with organic transistors show short-term and long-term plasticity with electrical and optical stimuli[85]. ReRAM can also be realized by embedding QDs and metal nanoparticles into an organic or inorganic matrix. In particular, printed multi-level ReRAM has

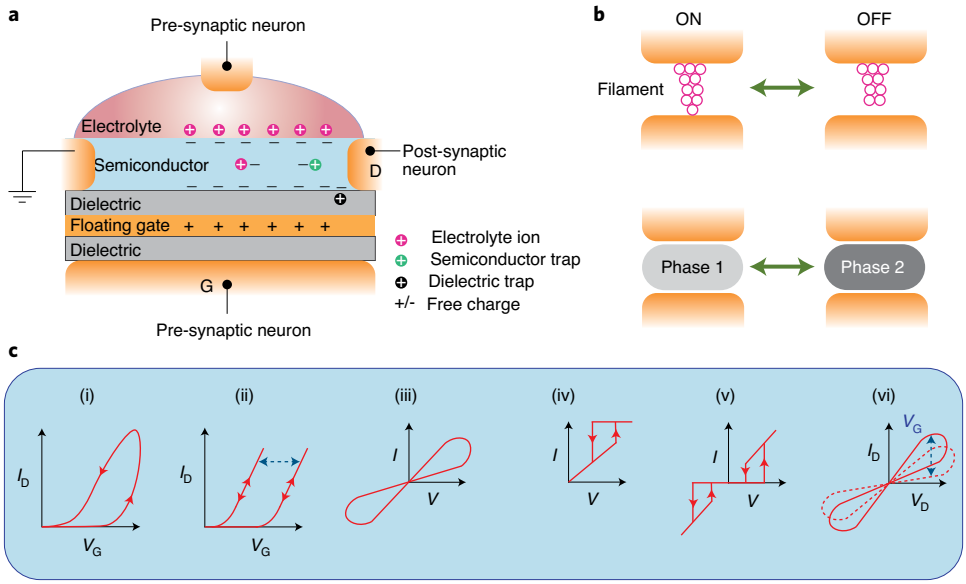

Fig. 1 | Synaptic transistors and memristive systems. a, Schematic of an artificial synapse based on charge trapping, a floating gate, doping or redox mechanisms that are used in distinct devices but shown here in the same device for conciseness. Gate electrodes connect with pre-synaptic neurons (writing) and drain/source electrodes connect with post-synaptic neurons (reading). **b**, Schematics showing memristive switching by filament formation and rupture (top) or phase change (bottom). **c**, Schematics of current–voltage (*I*–*V*) characteristics of synaptic transistors and memristors. (i) Transfer characteristics (drain current, I_D, versus gate bias, V_G) of a synaptic transistor showing hysteresis. (ii) The threshold voltage of a synaptic transistor is controlled through a floating gate or redox reactions. (iii) A pinched hysteresis loop in the *I*–*V* characteristics of a two-terminal memristor. (iv) Unipolar threshold switching showing a hysteresis loop at higher biases. (v) Complementary resistive switching that can be realized by connecting two memristors. (vi) Gate-tunable pinched hysteresis loop in a memtransistor.

been realized with high switching ratio (~10^7) by sandwiching black phosphorus QDs within poly(methyl methacrylate) bilayers, where charge trapping in QDs assists filament formation and rupture[86]. Similar charge trapping in Au nanoparticles assembled on pentacene films has been exploited in synaptic transistors[87]. In some contexts, small molecules (for example, metal-coordinated azo-aromatics) also show advantageous 0D properties that compete with commercial inorganic ReRAM metrics (endurance ~10^{12} cycles, speed ~30 ns, footprint ~60 nm^2)[88]. Furthermore, while memristor filaments often approach nanoscale dimensions that ultimately show 0D character, the diffusive memristor is an explicit example of 0D Ag nanoparticles being intentionally embedded into a SiO_x matrix[67]. These Ag nanoparticles show dynamic contraction and extension due to competing effects of surface tension and electric field, resulting in effective learning behaviour.

Semiconducting QDs also provide opportunities for quantum memristors based on Josephson junctions where the phase difference between quasi-particles acts as a state variable[50,89]. These devices have the potential to eliminate stochasticity that is pervasive in conventional defect-based memristors, although the memristive loop is expected to be relatively small. Quantum neural networks and other neuromorphic architectures have also been proposed based on QD arrays[90,91]. In the context of fabrication challenges, metal oxide memristors have been scaled down to sub-5 nm channels with small pitch (~6 nm) that resembles the required QD array architecture[57]. However, the ultimate realization of a quantum neural network requires quantum coherence between QDs in addition to the required quantum states being realized in high-mobility semiconductors as opposed to metal oxides[91].

One-dimensional neuromorphic nanomaterials

Early interest in 1D nanomaterials for neuromorphic applications was motivated by their topological resemblance to tubular axons that is essential for hyper-connectivity in biological systems. In addition, 1D nanomaterials possess several attributes that can be exploited in devices including diverse physical and chemical properties, versatile bottom-up growth, and solution-processability. One of the most widely studied 1D nanomaterials is the carbon nanotube (CNT), which is a rolled-up graphitic cylinder with metallic or semiconducting behaviour depending on its chiral vector. With high charge carrier mobilities and favourable scaling properties, semiconducting single-walled CNTs have been pursued for post-silicon digital logic, particularly in the ultrashort channel limit (that is, sub-5 nm node)[28,92]. Synaptic circuits have also been considered using CNT transistor models[93]. However, due to challenges in achieving wafer-scale assembly and alignment of individual CNTs, significantly more effort has been applied to CNT network thin-film transistors (TFTs)[28].

CNT TFTs have been explored in two major classes of neuromorphic applications, namely synaptic transistors and integration of TFT logic with conventional memristors (CNT-based memristors are rare)[27]. Synaptic transistors have been demonstrated using aligned arrays of CNTs[38] and random networks of CNTs[39,94–98]. The underlying physical mechanisms in these devices include electrostatic modulation from a floating gate[39], charge trapping in oxide dielectrics[38,94,95] and ion-migration and electric double layer effects in polymer dielectrics[96,97]. CNT TFTs provide two benefits over competing approaches to synaptic transistors. First, the high local electric fields produced by the large curvature of CNTs assist in overcoming activation energies for charge trapping in deeper levels (Fig. 3a). Second, since CNT TFTs can be doped p-type or n-type, complementary inverters have been fabricated that allow conversion of relative timing information into pulse amplitudes, which simplifies the realization of STDP.[39] Furthermore, recent work on self-aligned T-gates on aligned CNT networks has facilitated scaling (channel length ~1 μm) and high-speed synaptic activities (pulse width ~2 μs)[38]. These CNT synaptic responses have also been used for unsupervised learning in a SNN model (Fig. 3b)[38]. However,

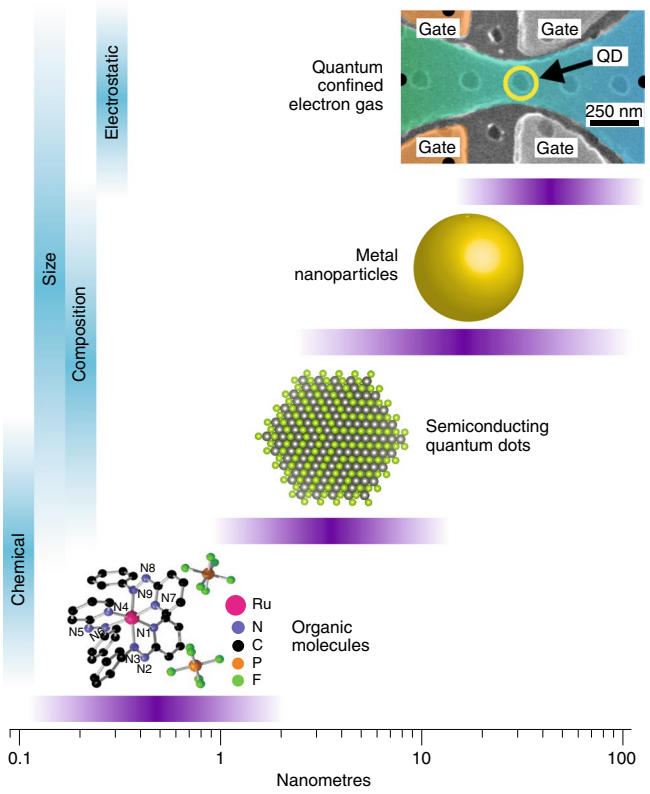

Fig. 2 | Zero-dimensional nanomaterials for electronic and optoelectronic synapses. Schematic of zero-dimensional nanomaterials used for neuromorphic computing. The organic molecule on the bottom left is a *mer*-$[Ru(L)_3](PF_6)_2$ complex with three bidentate ligands (L = 2(phenylazo) pyridine) each containing one azo (N = N) functional group (i.e., N2 = N3, N5 = N6 and N8 = N9). The semiconducting quantum dot crystal structure is for PbS. The quantum confined electron gas on the top right is achieved in an InAs quantum dot (QD) grown on a GaAs/AlGaAs heterostructure. Horizontal bars show typical ranges of physical dimensions, and vertical bars show the most relevant means of controlling properties for neuromorphic computing. Organic molecule schematic reproduced with permission from ref. [88], Springer Nature Ltd; quantum confined electron gas micrograph reproduced with permission from ref. [84], AIP.

remaining issues in CNT synaptic transistors include the lack of NVM and an intrinsically lateral geometry that prevents dense crossbar arrays. To circumvent these limitations, CNT TFTs have been integrated as logic units with vertical metal oxide memristors as NVM and silicon logic in a 3D architecture (Fig. 3c)[27]. Since their electronic properties are highly sensitive to adsorbates, CNT TFTs can also provide sensing functionality to underlying neuromorphic nanosystems[27].

Semiconducting nanowires constitute another broad class of 1D nanomaterials, which possess similar attributes to CNTs with some exceptions. Early neuromorphic research in group-IV and III–V semiconducting nanowires demonstrated NVM, which was activated by physisorbed redox molecules[99]. Charge trapping mechanisms have also been exploited in hybrid 1D–0D memristors based on vertically aligned ZnO nanowires decorated with CeO_2 QDs[100]. Similarly, Ag-contacted ZnO nanowires show diffusion of Ag atoms along the nanowire, which results in both volatile and non-volatile resistive switching, similar to Ag-SiO_x diffusive memristors (Fig. 3d)[67,101]. A wide range of additional inorganic 1D nanomaterials have been explored (for example, TiO_2, CuO_x, Cu_2O, NiO, Co_3O_4, Zn_2SnO_4, Ga_2O_3, Ag and Cu nanowires) with TiO_2 nanowires being particularly noteworthy since they show photo-electrosensitive mem-diode behaviour due to dynamic modulation of Schottky barrier heights from charge trapping and de-trapping near contacts[102,103]. In contrast, organic core-sheath (PEO-P3HT) nanowires not only emulate the morphology of biological nerve fibres but also possess learning mechanisms that resemble biological ion channels[104]. Here, pre-synaptic spikes assist electrolyte ion diffusion into the PEO sheath after which these ions diffuse back slowly, resulting in short-term potentiation. More persistent spikes drive ion penetration deeper into the P3HT core, which minimizes reverse diffusion, producing long-term potentiation with exceptionally low energy of ~10 fJ per event (Fig. 3e)[104]. More exotic neural networks have also been proposed for 1D nanowires such as a photonic system consisting of semiconducting light-emitting nanowires and superconducting nanowire-based single-photon detectors that have the potential to achieve low power densities (1 mW cm^{-2}) (Fig. 3f)[105].

In the context of neuromorphic applications, polymers similarly possess 1D characteristics in addition to mechanical flexibility, chemical sensitivity and biocompatibility that has been exploited in memristors (Fig. 3g) and organic electrochemical transistors (OECTs) (Fig. 3h). Since the earlier work on polymer resistive memories and OECTs have been reviewed extensively elsewhere[36,37,59,106], we limit our discussion to more recent work where the 1D nature of polymers has enabled neuromorphic functionality. For example, memristors based on polyelectrolyte brushes of poly(acrylic acid) covalently tethered to Au electrodes have shown tunable switching voltages through cation exchange with NH_4^+, $N(CH_3)_4^+$, Ag^+ and Na^+ ions (Fig. 3g)[107]. Polymers have also been employed for mechanically flexible NVMs including an all-organic 64-bit one-diode-one-resistor memory[108]. In addition, polymer OECTs have been utilized as synaptic transistors where 1D polymer chains serve as the conducting channel where charge transport is modulated by redox reactions that are driven by voltage pulses on the gate electrode (Fig. 3h)[37]. While polymer electrolytes have also been integrated with planar silicon and even lithium-ion battery materials to realize synaptic transistors[109,110], OECTs offer advantages since electrolyte ions penetrate deeper into polymer films, resulting in large capacitances that increase linearly with volume unlike the areal scaling of parallel plate capacitors. Consequently, OECTs show low energy consumption (~10 pJ per event) and can attain more than 500 distinct conductance states within a 1 V range (Fig. 3h,i)[111,112]. Moreover, since the common electrochemical environment created by the polymer electrolyte allows coupling with multiple gates in arbitrary geometries, the resulting spatially distributed gate inputs can achieve homeoplasticity that couples global and local activities in biological neural networks[113,114].

Two-dimensional neuromorphic nanomaterials

Fundamental research in 2D nanomaterials over the past decade has set the stage for several technologies, as reviewed elsewhere[29,30,115,116]. Compared to 0D and 1D nanomaterials, 2D nanomaterials provide improved device scaling and integration with planar wafer technology. Initial attempts to realize neuromorphic functionality in 2D nanomaterials revealed unexpected mechanisms that subsequently spurred the development of new device concepts. For example, monolayer transition metal dichalcogenides (TMDCs) of the form MX_2 (M = Mo, W; X = S, Se) sandwiched between Au electrodes have been incorporated into ultrathin vertical memristors (thickness < 1 nm) (Fig. 4a)[117,118], whose low ON-state resistance (<10 Ω) enables high-frequency switches that operate at 50 GHz[117]. Their high switching ratio (> 10^4) refutes conventional thinking concerning leakage currents in monolayer semiconductors, suggesting new switching mechanisms where point defects are likely playing a central role[118]. In related work, few-layer MoS_2 memristors sandwiched between graphene layers (that is, van der Waals contacts) have shown significantly higher operating temperatures (340 °C) than conventional metal oxide memristors (200 °C)[119]. In situ scanning

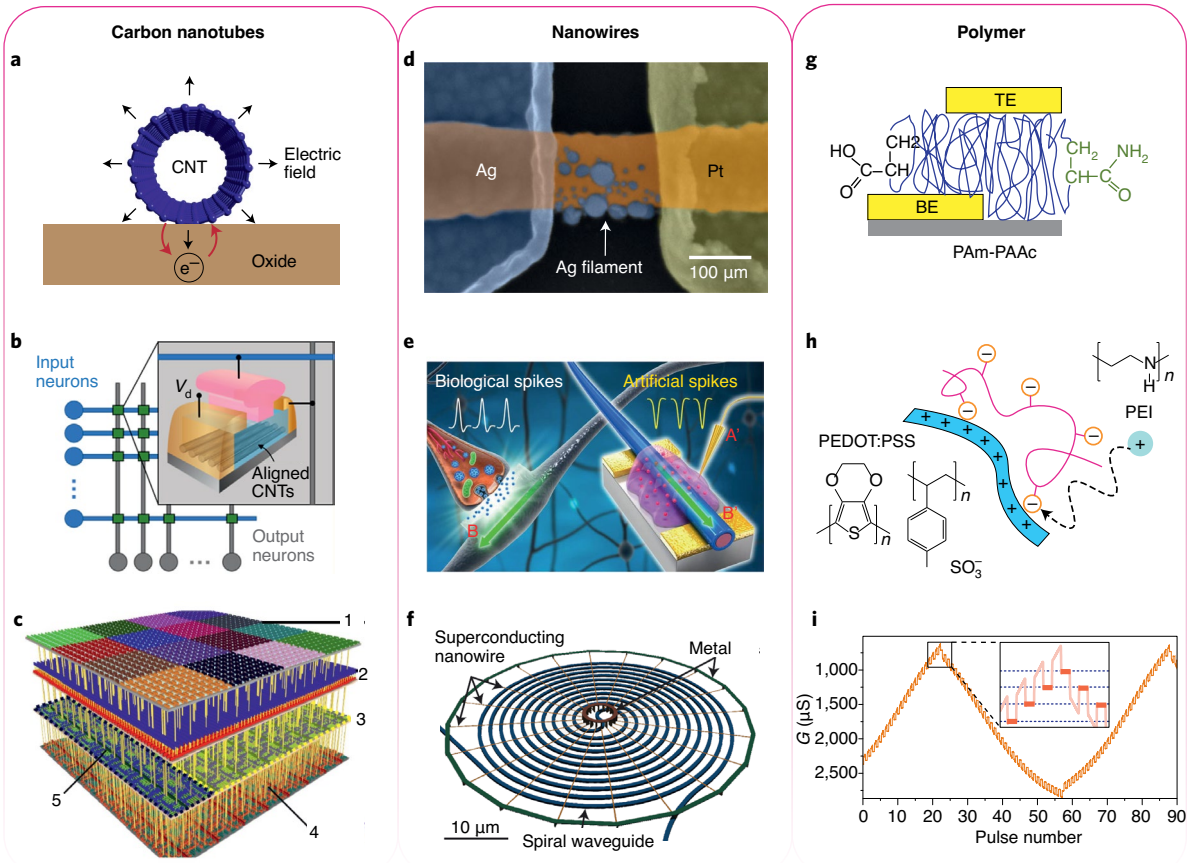

Fig. 3 | One-dimensional nanomaterials for neuromorphic circuits. a, A schematic showing electron tunnelling between a CNT and a charge trap in the neighbouring gate dielectric due to the large electric field that results from high CNT curvature. This type of charge trapping underlies the majority of CNT-based neuromorphic devices. **b**, A schematic showing the implementation of unsupervised learning for pattern recognition in a SNN using aligned CNT synaptic transistors. **c**, Illustration of a 3D-integrated CNT and Si transistor nanosystem for remote classification in gas sensing applications. The five labelled layers are: (1) CNT sensors as input, (2) ReRAM for memory, (3) CNT FET logic, (4) silicon logic and (5) ultra-dense interconnects. **d**, Scanning electron microscopy image (with false colour) of a single ZnO nanowire memristor contacted by Pt and electrochemically-active Ag electrodes. Ag atoms migrate along the nanowire to form a conducting filament. **e**, Schematic showing an electrolyte-gated organic nanowire (right, B') mimicking excitatory postsynaptic current in a biological synapse (left, B'). The gate probe A' mimics the axon. **f**, A proposed schematic for a spider web neuron based on a superconducting nanowire single-photon detector. **g**, Schematic of a vertical synaptic switch based on the block copolymer polyacrylamide (PAm) and poly(acrylic acid) (PAAc). TE, top electrode; BE, bottom electrode. **h**, Schematic of the redox reaction in an organic electrochemical transistor (OECT) where a free proton from the polyethylenimine (PEI) polymer alters the conductivity along the poly(3,4-ethylenedioxythiophene) polystyrene sulfonate (PEDOT:PSS) polymer backbone. **i**, Long-term potentiation of an OECT where discrete conduction levels are achieved by pre-synaptic pulses. Reproduced with permission from ref. [38], American Chemical Society (**b**); ref. [27], Springer Nature Ltd (**c**); ref. [101], distributed under a CC BY 4.0 license (https://creativecommons.org/licenses/by/4.0/) (**d**); ref. [105], APS (**f**); and ref. [111], Springer Nature Ltd (**i**). Panel **e** reprinted with permission from ref. [104], AAAS. © The Authors, some rights reserved; exclusive licensee American Association for the Advancement of Science. Distributed under a Creative Commons Attribution NonCommercial License 4.0 (CC BY-NC) http://creativecommons.org/licenses/by-nc/4.0/. Panel **g** adapted with permission from ref. [107], Springer Nature Ltd.

transmission electron microscopy of these memristors revealed an increased density of sulfur vacancies in the ON-state that are filled by oxygen ions in the OFF-state. On the other hand, bilayer MoS_2 memristors sandwiched between Cu and Au electrodes not only show low switching voltages (~0.2 V) that result from diffusion of Cu ions but also the first demonstration of STDP in 2D memristors using tailored pulse shapes[120]. Vertical memristors based on few-layer hexagonal boron nitride (hBN) have also demonstrated bipolar and unipolar resistive switching[121,122]. In this case, the hBN memristors are contacted by electrochemically active metals (Cu or Ag), resulting in switching due to the diffusion of metal ions through point defects as confirmed by conductive atomic force microscopy, electron microscopy and kinetic Monte-Carlo simulations[121–123].

Additional neuromorphic functionality has been realized using 2D nanomaterials in lateral device geometries. For instance, ambipolar graphene-based synaptic transistors show tunable plasticity where the polarity of Hebbian learning and STDP are controlled by gate voltage polarity[124]. In addition, lateral devices based on graphene oxide have shown non-zero-crossing hysteretic current–voltage characteristics, instead of a pinched hysteresis loop[125]. This behaviour can be attributed to activated polarization resulting from the migration of residual H^+ and SO_4^{2-} ions with the resulting synapses showing tunability as a function of the amplitude and frequency of periodic stimuli. The ability to host ion transport also enables graphene oxide to act as a solid-state ionic conductor for synaptic transistors based on indium zinc oxide semiconductors[126]. Similarly, the in-plane diffusion of Li^+ ions in graphene synapses allows for low power (<500 fJ per event) and multi-state memory (>250 states) that compete well with OECTs[111,127]. The out-of-plane ionic permeability of graphene through point defects has also

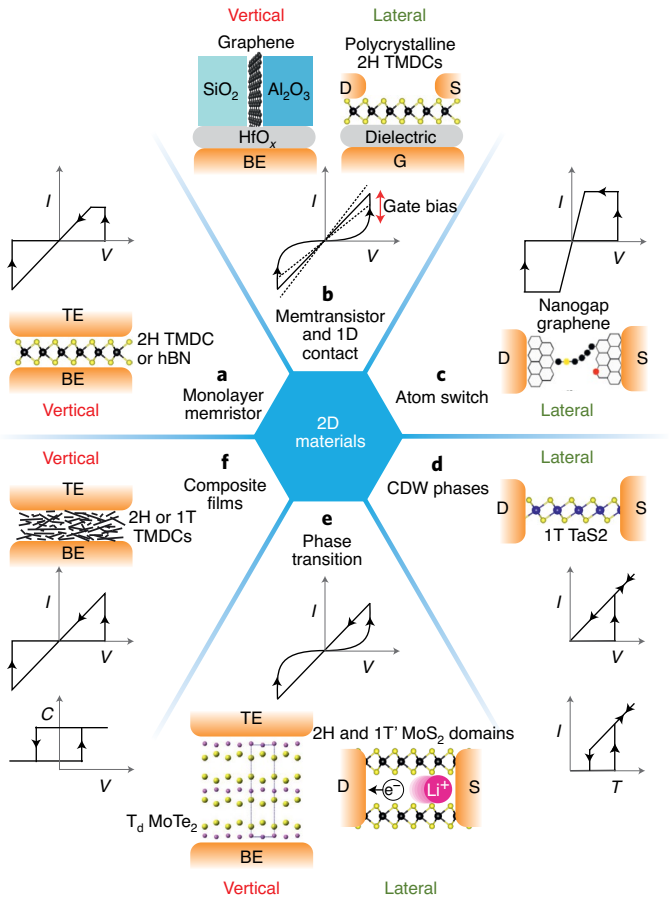

Fig. 4 | Memristive systems from 2D nanomaterials. a, Schematic and representative *I*–*V* characteristics of monolayer and ultrathin vertical memristors composed of TMDCs or hBN. **b**, Schematics of a vertical metal oxide memristor contacted by a graphene edge (left) and a lateral memtransistor (right) with gate-tunable *I*–*V* characteristics. D, drain electrode; S, source electrode; G, gate electrode. **c**, Schematic and *I*–*V* characteristics of a lateral atom switch based on a nanojunction in patterned graphene. **d**, Schematic of a lateral TaS_2 phase change memristor based on the transition from a commensurate to nearly commensurate charge density wave (CDW) phase. Both *I*–*V* and current–temperature (*I*–*T*) characteristics show hysteretic loops. **e**, Schematic of lateral and vertical phase change memristors and corresponding *I*–*V* characteristics. The lateral TMDC memristor relies on the semiconducting 2H to metallic 1T′ phase transition, whereas the vertical $MoTe_2$ memristor relies on the 2H to the T_d phase transition. **f**, Schematic, *I*–*V*, and capacitance–voltage (*C*–*V*) characteristics of a vertical memristor and memcapacitor fabricated from TMDC composite films. Bottom panel in **c** adapted with permission from ref. [142], American Chemical Society; left panel in **e** adapted with permission from ref. [144], Springer Nature Ltd.

been used to control the size of conducting filaments in cationic memristors[128]. Finally, 3D architectures of memory and logic have been realized by contacting memristors laterally through graphene edges (Fig. 4b)[129].

Synaptic transistors have also been explored using ionic motion in layered TMDCs and black phosphorus. For example, in-plane lithium-ion intercalation in few-layer WSe_2 showed significantly smaller energy consumption (~30 fJ per event) than graphene synapses and OECTs, and double floating gates on MoS_2 devices enabled superior linearity and symmetry[40,111,127,130]. These diffusive dynamics have been generalized to other 2D nanomaterials and polymer electrolyte dielectrics[35,131,132]. In addition, a correlated response from multiple stimuli (for example, electrical, ionic and optical) have enabled greater functionality such as on-demand symmetric and asymmetric Hebbian learning[131]. Since 2D nanomaterials possesses exceptionally high surface-to-volume ratios, they not only interact with oxide traps but also allow post-growth defect engineering for synaptic transistors and multi-level memory[133–135]. Due to its in-plane anisotropic electronic properties, black phosphorus further enables anisotropic synaptic responses[136]. Local thermal effects and weak electrostatic screening in 2D have also been exploited to encode interaural time difference for sound localization, although the device footprints present challenges for further circuit integration[34,137].

Passive crossbars with transistor selectors (that is, 1T1M) can relax the requirements for device uniformity by minimizing the sneak current through neighbouring cells[71], particularly during network training steps (although it is worth noting that the sneak current issue is alleviated during testing or inference steps)[25]. Separate layers of memristors and transistor selectors not only negatively impact integration density but also their processing steps are often not compatible. Therefore, it is of high interest to combine the desirable characteristics of a transistor and memristor into a single device. Such gate-tunable memristors (that is, memtransistors) were first conceptualized using silicon and metal oxide synaptic transistors[77]. More recently, gate-tunable memristive switching was observed in substoichiometric monolayer MoS_2 devices with individual grain boundaries in the channel[74]. However, the switching characteristics of these devices depend strongly on grain boundary topology, which may limit large-area uniformity. Thus, scalable memtransistor arrays were subsequently realized in polycrystalline MoS_2 with grain sizes that were much smaller than the channel area such that the effects of individual grain boundary geometries were averaged at the device level (Fig. 4b)[33,138]. The open architecture of the 2D channel further enabled multi-terminal heterosynaptic plasticity (Fig. 5b)[33]. While the initial devices possessed large operating voltages (>50 V), follow-up work reduced the operating voltage by an order of magnitude by using smaller grain sizes and ultrathin dielectrics[76]. Few-layer GaSe memtransistors have similarly shown high switching ratios in excess of 10^5 and low voltage operation down to 2 V. Post-growth defect engineering using helium-ion or electron-beam irradiation has also shown promise for tailoring the behaviour of MoS_2 memtransistors[139,140].

Other novel resistive switching concepts in 2D nanomaterials include atom switches and quantum phase transitions. Graphene-based atom switches involve the formation of a carbon chain in a nanogap that is formed by an applied electric field and subsequently ruptured by Joule heating (Fig. 4c)[141,142]. As an example of a quantum phase change memristor, few-layer 1T-TaS_2 showed a phase transition between an incommensurate charge density wave (CDW) to a nearly commensurate CDW at 350 K and another phase transition to the Mott state of a commensurate CDW between 100 K and 220 K depending on the temperature sweep direction (Fig. 4d)[143]. These CDW phase transitions result in hysteretic current–temperature curves and memristive current–voltage curves (Fig. 4d)[143], although this system is not yet competitive with NbO_2 Mott memristors and chalcogen-based phase-change materials for neuromorphic applications[13,65].

Recently, the 2H–1T' phase transition in few-layer MoS_2 has been used to achieve synaptic competition and synergy in multi-terminal devices (Fig. 4e)[35]. In this case, in addition to field-driven Li^+ ion intercalation that is similar to graphene synapses[40,127], the MoS_2 synapses also involve a local 2H–1T' phase change that is associated with dynamically varying ion density[35]. Vertical ReRAM has also been achieved using quantum phase transitions from semiconducting 2H to distorted $2H_d$ and orthorhombic T_d structures in $MoTe_2$ and $Mo_{1-x}W_xTe_2$ alloys (Figs. 4e, 5e)[144]. This field-driven phase change produces higher speed (~10 ns) and larger switching ratio

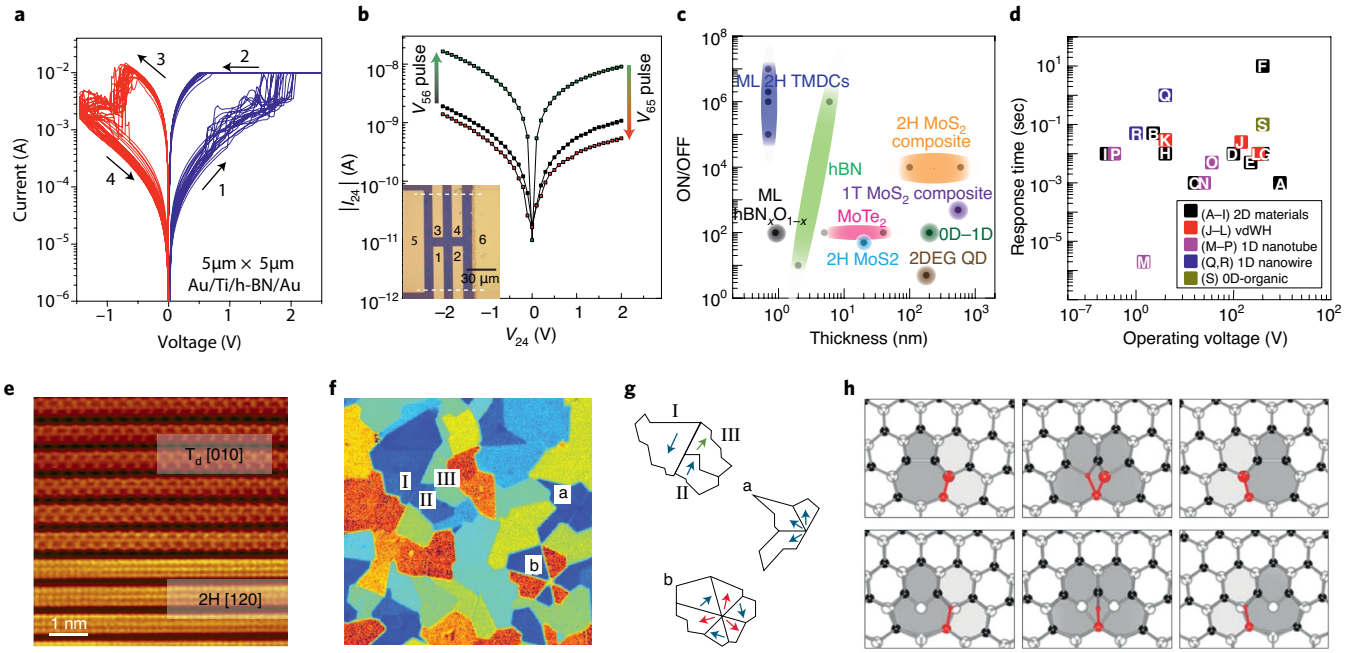

Fig. 5 | Device metrics and mechanisms. a, *I*–*V* characteristics of a few-layer hBN vertical memristor. **b**, *I*–*V* characteristics of a multi-terminal memtransistor (inset) showing heterosynaptic plasticity. The conductance between electrodes 2 and 4 (I_{24}/V_{24}) is modulated reversibly by applying pulses between electrodes 5 and 6 (V_{56}). **c**, Comparison plot of switching ratio (ON/OFF) versus channel thickness (length) for vertical (lateral) memristors realized from 0D, 1D, 2D and hybrid nanosystems. Sources: monolayer (ML) 2H TMDCs, ML hBN_xO_{1-x}, hBN, $MoTe_2$, 2H MoS_2, 2H MoS_2 composite, 1T MoS_2 composite, 0D–1D (CeO_2/ZnO) and 2D electron gas (2DEG) QD systems from refs. [100,118,119,121,123,144,146,147] and ref. [84], respectively. **d**, Comparison plot of response time versus operating voltage for synaptic transistors from 0D, 1D, 2D and van der Waals heterojunctions (vdWHs). Sources: data points A to S are taken from refs. [33,35,38,39,41,87,95,97,103,104,124,126,132,133,136,139,148,149,158], in that order. **e**, Atomic-resolution transmission electron microscopy image of a $MoTe_2$ memristor showing emergence of T_d (top) during switching and typical 2H phase (bottom). **f**, False-colour micrograph showing grain boundaries in a polycrystalline monolayer MoS_2 layer probed by second harmonic generation microscopy. **g**, Schematics of irregular-shaped polycrystalline aggregates from **f** showing different crystal orientations. **h**, Schematics showing the starting point (left), saddle-point (middle) and final configurations (right) for S5|7 (top panels) and S5|7 + *V*s (bottom panels) dislocations in monolayer MoS_2, respectively, as obtained from first principles calculations[156]. Reproduced with permission from ref. [122], Springer Nature Ltd (**a**); ref. [33], Springer Nature Ltd (**b**); ref. [144], Springer Nature Ltd (**e**); ref. [159], AAAS (**f**,**g**); and ref. [156], American Chemical Society (**h**).

(~10^6) than ion-intercalated devices. Finally, solution-processing of 2D materials has been explored for large-area, flexible and printable neuromorphic circuits[60,145], particularly for NVM[60]. For example, solution-processed 2H and 1T' MoS_2 films have been used in vertical memristors and memcapacitors that operate at low global fields ~10 kV cm^{-1} (Fig. 4f)[146,147].

Neuromorphic van der Waals heterostructures

Due to the van der Waals bonding between low-dimensional nanomaterials, diverse heterojunctions can be realized without the epitaxial constraints encountered in conventional compound semiconductor heterojunctions[30,116]. As discussed above, synaptic responses have been amplified by sensitizing 1D nanotubes and nanowires with 0D organic molecules (that is, mixed-dimensional 1D–0D heterojunctions). A similar concept has been shown in 2D–0D mixed-dimensional heterojunctions based on MoS_2 and perylene-3,4,9,10-tetracarboxylic dianhydride (PTCDA) heterojunctions[41]. However, the true novelty of van der Waals heterojunctions results from the gate tunability of response functions due to incomplete dielectric screening in low-dimensional nanomaterials. For example, the gate-tunable Fermi level in graphene that has been utilized in barristors[115] further enables tunability of potentiation in vertical graphene/WSe_2/WO_x heterojunctions[148]. Similarly, electric-field effects in heterojunctions based on black phosphorus and SnSe can tune band alignments in a manner that control STDP as a function of bias polarity[149].

Most of these examples are artificial synapses, which reveals the greater challenge of designing spiking neurons using memristive systems[65,67]. Furthermore, the stochastic nature of memristors introduces variability, although attempts have been made to use noise and chaos to overcome this limitation[65]. Although CMOS-based neurons are the most widely used currently[8], a nanomaterials-based approach has the potential to simplify circuit implementation. A deterministic neuron approach requires two ingredients—namely, positive feedback for spiking followed by negative feedback for discharge and a refractory period. In this regard, anti-ambipolar (that is, Gaussian) transistors provide positive and negative transconductances that can be exploited for positive and negative feedback. A diverse range of mixed-dimensional (0D–2D, 1D–2D, 1D–3D) van der Waals p–n heterojunctions has demonstrated such Gaussian characteristics, suggesting potential applications in spiking neurons[31,150–153]. Gaussian responses are further desired for other neuromorphic applications such as efficient image recognition algorithms[154]. Serial assemblies of n-type and p-type 2D transistors with appropriate threshold voltages can also result in Gaussian characteristics that have been used to implement probabilistic neural networks[155].

Mechanisms and technical challenges

In this section, we delineate the current understanding of mechanisms and technical challenges in nanomaterial-based neuromorphic devices. While size-dependent properties are a nearly ubiquitous theme in nanomaterial properties, its relevance in

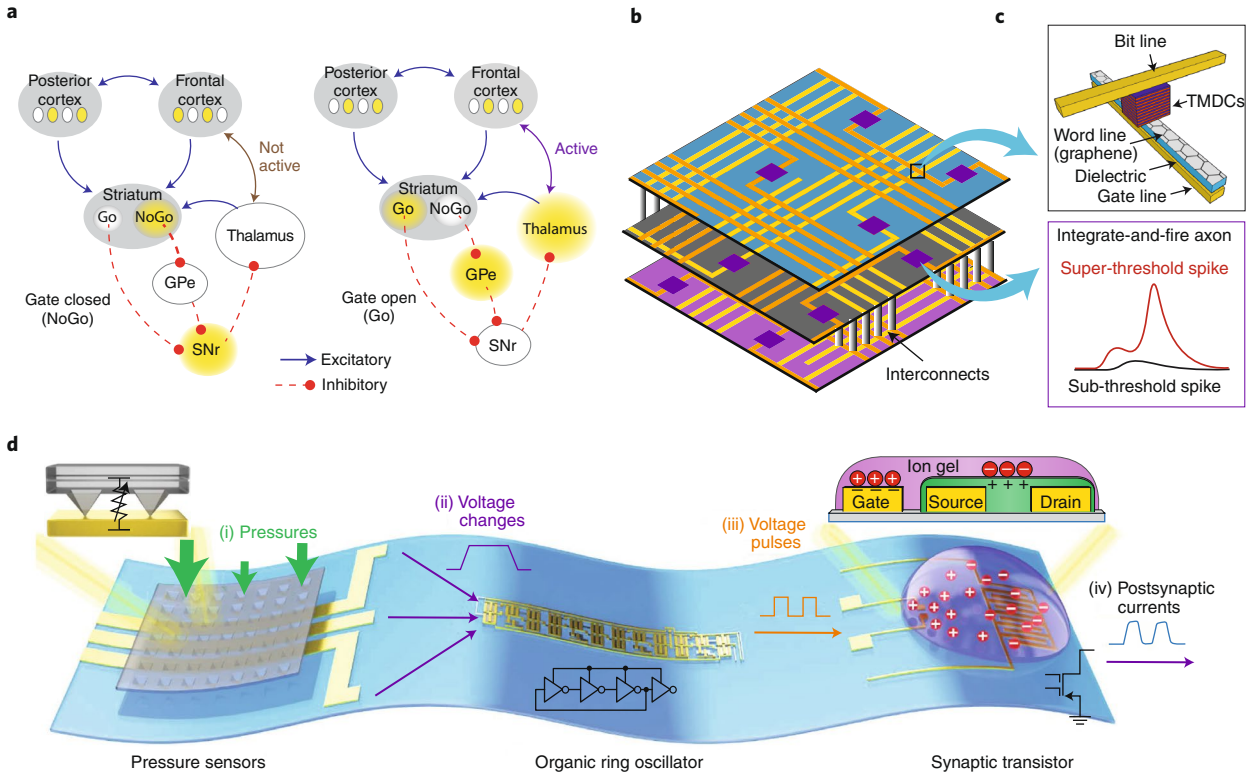

Fig. 6 | Biomimetic and biocompatible neuromorphic systems. a, Schematic showing the mechanism of two essential components of higher cognition — namely, robust active maintenance and rapid updating biological systems via dynamic gating. SNr, substantia nigra pars reticulata segment; GPe, globus pallidus external segment. **b**, Schematic of a 3D integrated circuit using multi-layered crossbar neural networks. **c**, Individual synapses and Hodgkin–Huxley axons are fabricated from gate-tunable vertical memristors (top) and volatile switching nanodevices (bottom), respectively. **d**, Schematic of an artificial afferent nerve consisting of pressure sensors, an organic ring oscillator and a synaptic transistor, all on a flexible substrate. Adapted with permission from ref. [164], AAAS (**a**) and reproduced with permission from ref. [42], AAAS (**d**).

neuromorphic devices is not straightforward. For example, the switching ratio in 2D memristors does not always scale with thickness and shows large variations due to competing switching mechanisms (Fig. 5c). Figure 5d further shows operating voltage and speed for a selected set of synaptic transistors discussed in the preceding sections where the operating voltages range from 0.3 V to 30 V with no clear correlation with speed or thickness. In addition, the response time is consistently larger than 1 millisecond, irrespective of material or device architecture, which can likely be attributed to most synaptic transistors involving the inherently slow processes of charge trapping or ion motion. Evidently, the device metrics in neuromorphic devices involve a complex set of factors that defy simple design rules, and thus a deep understanding of the underlying physical mechanisms is necessary to optimize a specific system.

Quantum phase change memristors (Fig. 5e) and QD photonic synapses are rare examples where switching mechanisms can be understood from first principles[82,143,144]. In contrast, filamentary switching and ion diffusion involve several co-dependent non-equilibrium phenomena involving electron transport, thermal effects and defect migration[10,50]. First-principles calculations provide some insight into fundamental defect dynamics (Fig. 5h)[76,156], but device-level switching mechanisms require molecular dynamics and kinetic Monte-Carlo simulations due to their size and complexity[123,157]. In this regard, nanomaterials present an open system for in situ characterization that helps guide theoretical insight. For example, in situ electrostatic force microscopy has revealed local potential profiles at grain boundaries and contacts in MoS_2 memtransistors[33,74]. Since Schottky barrier heights are influenced by local dopant density and sulfur vacancies serve as n-type dopants in MoS_2, spatially-resolved Auger electron spectroscopy has been employed to map the atomic percentages of Mo and S in the MoS_2 channel[158]. Alternative methods such as second harmonic generation (Fig. 5f,g), where grain boundary contrast originating from differing lattice symmetries is robust against local defects, may also reveal memristive switching mechanisms[156,159].

Integration of nanomaterials in neuromorphic circuits faces several challenges such as the need for improved device-to-device uniformity, high device density and low read currents in large crossbar arrays. To date, nanomaterials do not outperform conventional neuromorphic devices in all of these metrics concurrently, which implies that short-term opportunities need to be tolerant to design tradeoffs. For example, OECTs show impressive uniformity but poor integration density[37], whereas vertical memristors from monolayer 2D materials promise high integration density but lack the uniformity that has been achieved for state-of-the-art memristors[118]. Similarly, lateral synaptic transistors and memtransistors inherently possess a larger footprint than vertical memristors (albeit not worse than the 1T1M architecture), which suggests that their crossbar arrays are best suited for applications that require gate-tunability and non-Hebbian learning as opposed to ultra-dense NVM. Moreover, synaptic transistors based on CNT networks, 2D semiconductors and organic polymers are suitable for medium-scale nanosystems, where attributes such as mechanical resilience, sensing and processing flexibility are more important than ultrahigh density[27,42].

Conclusions

Nanomaterials are providing diverse opportunities in emerging neuromorphic devices and architectures. As the field evolves, a

holistic understanding of nanomaterial properties will be necessary to move beyond exploratory research and towards rational down-selection and refinement of the most promising candidates. In this regard, standardized material and device characterization protocols are being developed by the neuromorphic community[56]. In parallel, benchmarking, compact models and computational research are needed for nanoscale devices[4]. Ultimately, complete system-level demonstrations are necessary to expedite neuromorphic computing technologies since overall performance is the collective response of components and connections[160].

Close collaboration between neuroscientists, computer architects and materials scientists is crucial to realize the full potential of nanomaterials in neuromorphic devices and systems. In particular, the rapidly growing knowledge base in neuroscience is leading to unprecedented insight into the physiology of the mammalian brain, which can inform new concepts in neuromorphic computing. On the other hand, increasingly efficient ANN algorithms are emerging but deterministic relationships between overall efficiency and individual synaptic weights become unclear with more than two layers, which implies that the complexity of neuromorphic systems falls far short of biological analogues. Reconciliation of this dichotomy is a fertile ground for innovation in ANN algorithms that will inform future hardware implementations. For example, higher cognition in the human brain involves both active maintenance of information while also achieving rapid updates via dynamic gating mechanisms as shown in Fig. 6a. Specifically, NoGo neurons in the left schematic of Fig. 6a are constantly firing (gate closed) to maintain ongoing activity. However, when Go neurons fire (gate open) they disinhibit the excitatory loop through the thalamus and the frontal cortex, thus triggering a rapid update in the working memory (right schematic in Fig. 6a). In this context, nanomaterials will become increasingly relevant in the future since they allow tunability of responses encompassing Hebbian, non-Hebbian, competitive and homeostatic learning[1,2].

In addition, nanomaterials possess desirable form factors for 3D circuitry with synaptic hyper-connectivity at the device level that present opportunities beyond the 3D addressable topology schemes that currently exist for two-terminal memristor crossbar arrays[161]. Specifically, the open architecture of atomically thin 2D materials enables gate-tunability and multi-terminal synapses with heterosynaptic plasticity (Fig. 5b) that have the potential to facilitate 3D integration through stacked 2D layers and vertical interconnects (Fig. 6b)[33,35,74,76]. Gate-tunability also provides a pathway to the negative feedback loops that underlie non-Hebbian learning[58]. Towards this end, effective integration schemes are being developed for nanomaterials, including self-assembly of 0D and 1D nanomaterials and self-alignment schemes for 2D van der Waals heterostructures[28,150]. To circumvent scaling issues encountered with lateral synapses, gate-tunability in vertical barristor-like synapses can be achieved by using graphene contacts (Fig. 6c, top). Similarly, vertical integration of nanomaterials with conventional memristors provides a pathway to improved scaling. To exceed the performance of CMOS in neuromorphic architectures, nanomaterial-based implementations will require the development of neurons and synapses from the same or processing-compatible materials (Fig. 6c, bottom). In addition, the correlated processes (for example, electrical and thermal)[69] and degrees of freedom (for example, spin and valley) in emerging nanomaterials hold promise for realizing spiking behaviour that is significantly less developed than synaptic devices[29,30,162]. The additional chemical sensing, mechanical flexibility and biocompatibility attributes of nanomaterials provide further opportunities to realize edge computing and afferent neurons in artificial skin (Fig. 6d)[27,42,163]. In this manner, since the properties and reduced dimensionality of nanomaterials closely mimic biological systems, they possess significant potential for realizing neuromorphic computing systems that better emulate animate neural networks.

Received: 9 July 2019; Accepted: 23 January 2020;
Published online: 02 March 2020

References

1. Goodfellow, I., Bengio, Y. & Courville, A. *Deep Learning* (The MIT Press, 2016).
2. LeCun, Y., Bengio, Y. & Hinton, G. Deep learning. *Nature* **521**, 436–444 (2015).
3. James, C. D. et al. A historical survey of algorithms and hardware architectures for neural-inspired and neuromorphic computing applications. *Biol. Insp. Cog. Arch.* **19**, 49–64 (2017).
4. Schuman, C. D. et al. A survey of neuromorphic computing and neural networks in hardware. Preprint at https://arxiv.org/abs/1705.06963 (2018).
5. Bear, M. F., Connors, B. W. & Paradiso, M. A. *Neuroscience: Exploring the Brain* (Wolters Kluwer, 2015).
6. Indiveri, G., Chicca, E. & Douglas, R. J. Artificial cognitive systems: From VLSI networks of spiking neurons to neuromorphic cognition. *Cogn. Comp.* **1**, 119–127 (2009).
7. Indiveri, G. et al. Neuromorphic silicon neuron circuits. *Front. Neuro.* **5**, 73 (2011).
8. Krestinskaya, O., James, A. P. & Leon, C. O. Neuro-memristive circuits for edge computing: A review. *IEEE Trans. Neural Netw. Learn. Syst.* **31**, 4–23 (2020).
9. Jeong, D. S. et al. Memristors for energy-efficient new computing paradigms. *Adv. Elec. Mater.* **2**, 1600090 (2016).
10. Yang, J. J., Strukov, D. B. & Stewart, D. R. Memristive devices for computing. *Nat. Nanotechnol.* **8**, 13–24 (2013).
11. Merolla, P. A. et al. A million spiking-neuron integrated circuit with a scalable communication network and interface. *Science* **345**, 668–673 (2014).
12. Furber, S. B., Galluppi, F., Temple, S. & Plana, L. A. The SpiNNaker project. *Proc. IEEE* **102**, 652–665 (2014).
13. Tuma, T. et al. Stochastic phase-change neurons. *Nat. Nanotechnol.* **11**, 693–699 (2016).
14. Duygu, K., Shimeng, Y. & Wong, H. S. P. Synaptic electronics: materials, devices and applications. *Nanotechnology* **24**, 382001 (2013).
15. Wong, H. S. P. et al. Metal-oxide RRAM. *Proc. IEEE* **100**, 1951–1970 (2012).
16. Yu, S. & Chen, P. Y. Emerging memory technologies: Recent trends and prospects. *IEEE Sol. Stat. Circuit Mag.* **8**, 43–56 (2016).
17. Strukov, D. B., Snider, G. S., Stewart, D. R. & Williams, R. S. The missing memristor found. *Nature* **453**, 80–83 (2008).
18. Sengupta, A. & Roy, K. Neuromorphic computing enabled by physics of electron spins: Prospects and perspectives. *Appl. Phys. Exp.* **11**, 030101 (2018).
19. Prezioso, M. et al. Training and operation of an integrated neuromorphic network based on metal-oxide memristors. *Nature* **521**, 61–64 (2015).
20. Burr, G. W. et al. Neuromorphic computing using non-volatile memory. *Adv. Phys. X* **2**, 89–124 (2017).
21. Zidan, M. A., Strachan, J. P. & Lu, W. D. The future of electronics based on memristive systems. *Nat. Elect.* **1**, 22–29 (2018).
22. Wang, Z. et al. Fully memristive neural networks for pattern classification with unsupervised learning. *Nat. Electron.* **1**, 137–145 (2018).
23. Zidan, M. A. et al. A general memristor-based partial differential equation solver. *Nat. Electron.* **1**, 411–420 (2018).
24. Sun, Z. et al. Solving matrix equations in one step with cross-point resistive arrays. *Proc. Natl Acad. Sci. USA* **116**, 4123–4128 (2019).
25. Bayat, F. M. et al. Implementation of multilayer perceptron network with highly uniform passive memristive crossbar circuits. *Nat. Commun.* **9**, 2331 (2018).
26. Prezioso, M. et al. Spike-timing-dependent plasticity learning of coincidence detection with passively integrated memristive circuits. *Nat. Commun.* **9**, 5311 (2018).
27. Shulaker, M. M. et al. Three-dimensional integration of nanotechnologies for computing and data storage on a single chip. *Nature* **547**, 74–78 (2017).
28. Jariwala, D. et al. Carbon nanomaterials for electronics, optoelectronics, photovoltaics, and sensing. *Chem. Soc. Rev.* **42**, 2824–2860 (2013).
29. Jariwala, D. et al. Emerging device applications for semiconducting two-dimensional transition metal dichalcogenides. *ACS Nano* **8**, 1102–1120 (2014).
30. Sangwan, V. K. & Hersam, M. C. Electronic transport in two-dimensional materials. *Annu. Rev. Phys. Chem.* **69**, 299–325 (2018).
31. Jariwala, D., Marks, T. J. & Hersam, M. C. Mixed-dimensional van der Waals heterostructures. *Nat. Mater.* **16**, 170–181 (2016).
32. Upadhyay, N. K. et al. Emerging memory devices for neuromorphic computing. *Adv. Mater. Tech.* **4**, 1800589 (2019).
33. Sangwan, V. K. et al. Multi-terminal memtransistors from polycrystalline monolayer molybdenum disulfide. *Nature* **554**, 500–504 (2018).
34. Sun, L. et al. Synaptic computation enabled by Joule heating of single-layered semiconductors for sound localization. *Nano Lett.* **18**, 3229–3234 (2018).

35. Zhu, X., Li, D., Liang, X. & Lu, W. D. Ionic modulation and ionic coupling effects in MoS_2 devices for neuromorphic computing. *Nat. Mater.* **18**, 141–148 (2018).
36. van de Burgt, Y. et al. Organic electronics for neuromorphic computing. *Nat. Electron* **1**, 386–397 (2018).
37. Rivnay, J. et al. Organic electrochemical transistors. *Nat. Rev. Mater.* **3**, 17086 (2018).
38. Sanchez Esqueda, I. et al. Aligned carbon nanotube synaptic transistors for large-scale neuromorphic computing. *ACS Nano* **12**, 7352–7361 (2018).
39. Kim, S. et al. Pattern recognition using carbon nanotube synaptic transistors with an adjustable weight update protocol. *ACS Nano* **11**, 2814–2822 (2017).
40. Zhu, J. et al. Ion gated synaptic transistors based on 2D van der Waals crystals with tunable diffusive dynamics. *Adv. Mater.* **30**, 1800195 (2018).
41. Wang, S. et al. A MoS_2/PTCDA hybrid heterojunction synapse with efficient photoelectric dual modulation and versatility. *Adv. Mater.* **31**, 1806227 (2018).
42. Kim, Y. et al. A bioinspired flexible organic artificial afferent nerve. *Science* **360**, 998–1003 (2018).
43. Ziegler, M., Wenger, C., Chicca, E. & Kohlstedt, H. Tutorial: Concepts for closely mimicking biological learning with memristive devices: Principles to emulate cellular forms of learning. *J. Appl. Phys.* **124**, 152003 (2018).
44. McCulloch, W. S. & Pitts, W. A logical calculus of the ideas immanent in nervous activity. *Bull. Math. Biophys.* **5**, 115 (1943).
45. Rosenblatt, F. The perceptron: A probabilistic model for information storage and organization in the brain. *Psych. Rev.* **65**, 386–408 (1958).
46. Hertz, J., Krogh, A. & Palmer, R. G. *Introduction to the Theory of Neural Computation* (Westview Press, 1991).
47. Wasserman, P. D. *Neural Computing: Theory and Practice* (Van Nostrand Reinhold, 1965).
48. Hodgkin, A. L. & Huxley, A. F. A quantitative description of membrane current and its application to conduction and excitation in nerve. *J. Physio.* **117**, 500–544 (1952).
49. Leon, C. Memristor, Hodgkin–Huxley, and edge of chaos. *Nanotechnology* **24**, 383001 (2013).
50. Pershin, Y. V. & Di Ventra, M. Memory effects in complex materials and nanoscale systems. *Adv. Phys.* **60**, 145–227 (2011).
51. Rumelhart, D. E., Hinton, G. E. & Williams, R. J. Learning representations by back-propagating errors. *Nature* **323**, 533–536 (1986).
52. Minsky, M. *A Neural-Analogue Calculator Based Upon a Probability Model of Reinforcement* (Harvard University Psychological Laboratories, 1952).
53. Diorio, C., Hasler, P., Minch, A. & Mead, C. A. A single-transistor silicon synapse. *IEEE Trans. Electron. Dev.* **43**, 1972–1980 (1996).
54. Buonomano, D. V. & Maass, W. State-dependent computations: spatiotemporal processing in cortical networks. *Nat. Rev. Neurosci.* **10**, 113 (2009).
55. Qian, C. et al. Multi-gate organic neuron transistors for spatiotemporal information processing. *Appl. Phys. Lett.* **110**, 083302 (2017).
56. Lanza, M. et al. Recommended methods to study resistive switching devices. *Adv. Elec. Mater.* **5**, 1800143 (2019).
57. Pi, S. et al. Memristor crossbar arrays with 6-nm half-pitch and 2-nm critical dimension. *Nat. Nanotechnol.* **14**, 35–39 (2018).
58. Seok, J. Y. et al. A review of three-dimensional resistive switching cross-bar array memories from the integration and materials property points of view. *Adv. Funct. Mater.* **24**, 5316–5339 (2014).
59. Waser, R., Dittmann, R., Staikov, G. & Szot, K. Redox-based resistive switching memories – Nanoionic mechanisms, prospects, and challenges. *Adv. Mater.* **21**, 2632–2663 (2009).
60. Tan, C., Liu, Z., Huang, W. & Zhang, H. Non-volatile resistive memory devices based on solution-processed ultrathin two-dimensional nanomaterials. *Chem. Soc. Rev.* **44**, 2615–2628 (2015).
61. Yang, J. J. et al. Memristive switching mechanism for metal/oxide/metal nanodevices. *Nat. Nanotechnol.* **3**, 429–433 (2008).
62. Pickett, M. D., Medeiros-Ribeiro, G. & Williams, R. S. A scalable neuristor built with Mott memristors. *Nat. Mater.* **12**, 114–117 (2013).
63. Chang, S. et al. Occurrence of both unipolar memory and threshold resistance switching in a NiO film. *Phys. Rev. Lett.* **102**, 026801 (2009).
64. Linn, E., Rosezin, R., Kugeler, C. & Waser, R. Complementary resistive switches for passive nanocrossbar memories. *Nat. Mater.* **9**, 403–406 (2010).
65. Kumar, S., Strachan, J. P. & Williams, R. S. Chaotic dynamics in nanoscale NbO_2 Mott memristors for analogue computing. *Nature* **548**, 318–321 (2017).
66. Wang, Z. et al. Capacitive neural network with neuro-transistors. *Nat. Commun.* **9**, 3208 (2018).
67. Wang, Z. et al. Memristors with diffusive dynamics as synaptic emulators for neuromorphic computing. *Nat. Mater.* **16**, 101–108 (2017).
68. Chua, L. O. & Sung, Mo,K. Memristive devices and systems. *Proc. IEEE* **64**, 209–223 (1976).
69. Abdelouahab, M.-S., Lozi, R. & Chua, L. Memfractance: A mathematical paradigm for circuit elements with memory. *Intern. J. Bifur. Chaos Appl. Sci. Engrg.* **24**, 1430023 (2014).
70. Kim, S. et al. Experimental demonstration of a second-order memristor and its ability to biorealistically implement synaptic plasticity. *Nano Lett.* **15**, 2203–2211 (2015).
71. Xia, Q. et al. Two- and three-terminal resistive switches: Nanometer-scale memristors and memistors. *Adv. Funct. Mater.* **21**, 2660–2665 (2011).
72. Yang, Y., Chen, B. & Lu, W. D. Memristive physically evolving networks enabling the emulation of heterosynaptic plasticity. *Adv. Mater.* **27**, 7720–7727 (2015).
73. Schultz, W. Predictive reward signal of dopamine neurons. *J. Neurophysio.* **80**, 1–27 (1998).
74. Sangwan, V. K. et al. Gate-tunable memristive phenomena mediated by grain boundaries in single-layer MoS_2. *Nat. Nanotechnol.* **10**, 403–406 (2015).
75. Yang, Y. et al. Three-terminal memtransistors based on two-dimensional layered gallium selenide nanosheets for potential low-power electronics applications. *Nano Energy* **57**, 566–573 (2019).
76. Wang, L. et al. Artificial synapses based on multiterminal memtransistors for neuromorphic application. *Adv. Funct. Mater.* **29**, 1901106 (2019).
77. Mouttet, B. Memristive systems analysis of 3-terminal devices. In *Proc. 2010 17th IEEE International Conference on Electronics, Circuits and Systems* 930–933 (IEEE, 2010).
78. Caporale, N. & Dan, Y. Spike timing–dependent plasticity: A Hebbian learning rule. *Ann. Rev. Neuro.* **31**, 25–46 (2008).
79. Bi, G.-q & Poo, M.-m Synaptic modifications in cultured hippocampal neurons: Dependence on spike timing, synaptic strength, and postsynaptic cell type. *J. Neuro.* **18**, 10464–10472 (1998).
80. Sun, C. et al. Single-chip microprocessor that communicates directly using light. *Nature* **528**, 534–538 (2015).
81. Lin, X. et al. All-optical machine learning using diffractive deep neural networks. *Science* **361**, 1004–1008 (2018).
82. Mesaritakis, C., Kapsalis, A., Bogris, A. & Syvridis, D. Artificial neuron based on integrated semiconductor quantum dot mode-locked lasers. *Sci. Rep.* **6**, 39317 (2016).
83. Maier, P. et al. Electro-photo-sensitive memristor for neuromorphic and arithmetic computing. *Phys. Rev. Appl.* **5**, 054011 (2016).
84. Maier, P. et al. Memristive operation mode of a site-controlled quantum dot floating gate transistor. *Appl. Phys. Lett.* **106**, 203501 (2015).
85. Wang, Y. et al. Photonic synapses based on inorganic perovskite quantum dots for neuromorphic computing. *Adv. Mater.* **30**, 1802883 (2018).
86. Han, S.-T. et al. Black phosphorus quantum dots with tunable memory properties and multilevel resistive switching characteristics. *Adv. Sci.* **4**, 1600435 (2017).
87. Alibart, F. et al. An organic nanoparticle transistor behaving as a biological spiking synapse. *Adv. Funct. Mater.* **20**, 330–337 (2010).
88. Goswami, S. et al. Robust resistive memory devices using solution-processable metal-coordinated azo aromatics. *Nat. Mater.* **16**, 1216–1224 (2017).
89. Chua, L. O. Nonlinear circuit foundations for nanodevices. I. The four-element torus. *Proc. IEEE* **91**, 1830–1859 (2003).
90. Roychowdhury, V. P., Janes, D. B., Bandyopadhyay, S. & Xiaodong, W. Collective computational activity in self-assembled arrays of quantum dots: a novel neuromorphic architecture for nanoelectronics. *IEEE Trans. Electron. Dev.* **43**, 1688–1699 (1996).
91. Altaisky, M. V. et al. Towards a feasible implementation of quantum neural networks using quantum dots. *Appl. Phys. Lett.* **108**, 103108 (2016).
92. Cao, Q. et al. Carbon nanotube transistors scaled to a 40-nanometer footprint. *Science* **356**, 1369–1372 (2017).
93. Joshi, J., Parker, A. C. & Hsu, C. A carbon nanotube cortical neuron with spike-timing-dependent plasticity. In *Proc. 2009 Annual International Conference of the IEEE Engineering in Medicine and Biology Society* 1651–1654 (IEEE, 2009).
94. Kim, S., Yoon, J., Kim, H.-D. & Choi, S.-J. Carbon nanotube synaptic transistor network for pattern recognition. *ACS Appl. Mater. Inter.* **7**, 25479–25486 (2015).
95. Shen, A. M. et al. Analog neuromorphic module based on carbon nanotube synapses. *ACS Nano* **7**, 6117–6122 (2013).
96. Kim, K. et al. A carbon nanotube synapse with dynamic logic and learning. *Adv. Mater.* **25**, 1693–1698 (2013).
97. Feng, P. et al. Printed neuromorphic devices based on printed carbon nanotube thin-film transistors. *Adv. Funct. Mater.* **27**, 1604447 (2017).
98. Danesh, C. D. et al. Synaptic resistors for concurrent inference and learning with high energy efficiency. *Adv. Mater.* **31**, 1808032 (2019).
99. Duan, X., Huang, Y. & Lieber, C. M. Nonvolatile memory and programmable logic from molecule-gated nanowires. *Nano Lett.* **2**, 487–490 (2002).
100. Younis, A. et al. High-performance nanocomposite based memristor with controlled quantum dots as charge traps. *ACS Appl. Mater. Inter.* **5**, 2249–2254 (2013).
101. Milano, G. et al. Self-limited single nanowire systems combining all-in-one memristive and neuromorphic functionalities. *Nat. Commun.* **9**, 5151 (2018).

102. Hong, D. S., Chen, Y. S., Sun, J. R. & Shen, B. G. Ternary synaptic plasticity arising from memdiode behavior of TiO_x single nanowires. *Adv. Elec. Mater.* **2**, 1500359 (2016).
103. O'Kelly, C. J. et al. Associative enhancement of time correlated response to heterogeneous stimuli in a neuromorphic nanowire device. *Adv. Elec. Mater.* **2**, 1500458 (2016).
104. Xu, W., Min, S.-Y., Hwang, H. & Lee, T.-W. Organic core-sheath nanowire artificial synapses with femtojoule energy consumption. *Sci. Adv.* **2**, e1501326 (2016).
105. Shainline, J. M., Buckley, S. M., Mirin, R. P. & Nam, S. W. Superconducting optoelectronic circuits for neuromorphic computing. *Phys. Rev. Appl.* **7**, 034013 (2017).
106. Cho, B. et al. Organic resistive memory devices: Performance enhancement, integration, and advanced architectures. *Adv. Funct. Mater.* **21**, 2806–2829 (2011).
107. Zhitenev, N. B., Sidorenko, A., Tennant, D. M. & Cirelli, R. A. Chemical modification of the electronic conducting states in polymer nanodevices. *Nat. Nanotechnol.* **2**, 237–242 (2007).
108. Ji, Y. et al. Flexible and twistable non-volatile memory cell array with all-organic one diode–one resistor architecture. *Nat. Commun.* **4**, 2707 (2013).
109. Lai, Q. et al. Ionic/electronic hybrid materials integrated in a synaptic transistor with signal processing and learning functions. *Adv. Mater.* **22**, 2448–2453 (2010).
110. Fuller, E. J. et al. Li-ion synaptic transistor for low power analog computing. *Adv. Mater.* **29**, 1604310 (2017).
111. van de Burgt, Y. et al. A non-volatile organic electrochemical device as a low-voltage artificial synapse for neuromorphic computing. *Nat. Mater.* **16**, 414–418 (2017).
112. Fuller, E. J. et al. Parallel programming of an ionic floating-gate memory array for scalable neuromorphic computing. *Science* **364**, 570–574 (2019).
113. Gkoupidenis, P. et al. Orientation selectivity in a multi-gated organic electrochemical transistor. *Sci. Rep.* **6**, 27007 (2016).
114. Gkoupidenis, P., Koutsouras, D. A. & Malliaras, G. G. Neuromorphic device architectures with global connectivity through electrolyte gating. *Nat. Commun.* **8**, 15448 (2017).
115. Castro Neto, A. H. et al. The electronic properties of graphene. *Rev. Mod. Phys.* **81**, 109–162 (2009).
116. Grigorieva, I. V. & Geim, A. K. Van der Waals heterostructures. *Nature* **499**, 419–425 (2013).
117. Kim, M. et al. Zero-static power radio-frequency switches based on MoS_2 atomristors. *Nat. Commun.* **9**, 2524 (2018).
118. Ge, R. et al. Atomristor: Nonvolatile resistance switching in atomic sheets of transition metal dichalcogenides. *Nano Lett.* **18**, 434–441 (2018).
119. Wang, M. et al. Robust memristors based on layered two-dimensional materials. *Nat. Elect.* **1**, 130–136 (2018).
120. Xu, R. et al. Vertical MoS_2 double-layer memristor with electrochemical metallization as an atomic-scale synapse with switching thresholds approaching 100 mV. *Nano Lett.* **19**, 2411–2417 (2019).
121. Pan, C. et al. Coexistence of grain-boundaries-assisted bipolar and threshold resistive switching in multilayer hexagonal boron nitride. *Adv. Funct. Mater.* **27**, 1604811 (2017).
122. Shi, Y. et al. Electronic synapses made of layered two-dimensional materials. *Nat. Elect.* **1**, 458–465 (2018).
123. Zhao, H. et al. Atomically thin femtojoule memristive device. *Adv. Mater.* **29**, 1703232 (2017).
124. Tian, H. et al. Graphene dynamic synapse with modulatable plasticity. *Nano Lett.* **15**, 8013–8019 (2015).
125. Wang, L. et al. Controllable multiple depression in a graphene oxide artificial synapse. *Adv. Elec. Mater.* **3**, 1600244 (2017).
126. Wan, C. J. et al. Flexible metal oxide/graphene oxide hybrid neuromorphic transistors on flexible conducting graphene substrates. *Adv. Mater.* **28**, 5878–5885 (2016).
127. Sharbati, M. T. et al. Low-power, electrochemically tunable graphene synapses for neuromorphic computing. *Adv. Mater.* **30**, 1802353 (2018).
128. Zhao, X. et al. Breaking the current-retention dilemma in cation-based resistive switching devices utilizing graphene with controlled defects. *Adv. Mater.* **30**, 1705193 (2018).
129. Lee, S. et al. Metal oxide-resistive memory using graphene-edge electrodes. *Nat. Commun.* **6**, 8407 (2015).
130. Yi, S.-G. et al. Artificial synaptic emulators based on MoS_2 flash memory devices with double floating gates. *ACS Appl. Mater. Inter.* **10**, 31480–31487 (2018).
131. John, R. A. et al. Synergistic gating of electro-iono-photoactive 2D chalcogenide neuristors: Coexistence of Hebbian and homeostatic synaptic metaplasticity. *Adv. Mater.* **30**, 1800220 (2018).
132. Jiang, J. et al. 2D MoS_2 neuromorphic devices for brain-like computational systems. *Small* **13**, 1700933 (2017).
133. Arnold, A. J. et al. Mimicking neurotransmitter release in chemical synapses via hysteresis engineering in MoS_2 transistors. *ACS Nano* **11**, 3110–3118 (2017).
134. Chen, M. et al. Abnormal multiple charge memory states in exfoliated few-layer WSe_2 transistors. *ACS Nano* **11**, 1091–1102 (2017).
135. He, G. et al. Thermally assisted nonvolatile memory in monolayer MoS_2 transistors. *Nano Lett.* **16**, 6445–6451 (2016).
136. Tian, H. et al. Anisotropic black phosphorus synaptic device for neuromorphic applications. *Adv. Mater.* **28**, 4991–4997 (2016).
137. Das, S., Dodda, A. & Das, S. A biomimetic 2D transistor for audiomorphic computing. *Nat. Commun.* **10**, 3450 (2019).
138. Sangwan, V. K., Lee, H.-S. & Hersam, M. C. Gate-tunable memristors from monolayer MoS_2. In *Proc. 2017 IEEE International Electron Devices Meeting* 5.1.1–514 (IEEE, 2017).
139. Jadwiszczak, J. et al. Neuromorphic MoS_2 memtransistors fabricated by localized helium ion beam irradiation. *ACS Nano* **13**, 14262–14273 (2019).
140. Xie, X. et al. Room temperature 2D memristive transistor with optical short-term plasticity. In *Proc. 2017 IEEE International Electron Devices Meeting* 5.3.1–534 (IEEE, 2017).
141. Standley, B. et al. Graphene-based atomic-scale switches. *Nano Lett.* **8**, 3345–3349 (2008).
142. Sarwat, S. G. et al. Scaling limits of graphene nanoelectrodes. *Nano Lett.* **17**, 3688–3693 (2017).
143. Yoshida, M. et al. Memristive phase switching in two-dimensional 1T-TaS_2 crystals. *Sci. Adv.* **1**, 1500606 (2015).
144. Zhang, F. et al. Electric-field induced structural transition in vertical $MoTe_2$- and $Mo_{1-x}W_xTe_2$-based resistive memories. *Nat. Mater.* **18**, 55–61 (2019).
145. Kang, J., Sangwan, V. K., Wood, J. D. & Hersam, M. C. Solution-based processing of monodisperse two-dimensional nanomaterials. *Acc. Chem. Res.* **50**, 943–951 (2017).
146. Cheng, P., Sun, K. & Hu, Y. H. Memristive behavior and ideal memristor of 1T phase MoS_2 nanosheets. *Nano Lett.* **16**, 572–576 (2016).
147. Bessonov, A. A. et al. Layered memristive and memcapacitive switches for printable electronics. *Nat. Mater.* **14**, 199–204 (2015).
148. Huh, W. et al. Synaptic barristor based on phase-engineered 2D heterostructures. *Adv. Mater.* **30**, 1801447 (2018).
149. Tian, H. et al. Emulating bilingual synaptic response using a junction-based artificial synaptic device. *ACS Nano* **11**, 7156–7163 (2017).
150. Sangwan, V. K. et al. Self-aligned van der Waals heterojunction diodes and transistors. *Nano Lett.* **18**, 1421–1427 (2018).
151. Jariwala, D. et al. Hybrid, gate-tunable, van der Waals p-n heterojunctions from pentacene and MoS_2. *Nano Lett.* **16**, 497–503 (2016).
152. Jariwala, D. et al. Large-area, low-voltage, antiambipolar heterojunctions from solution-processed semiconductors. *Nano Lett.* **15**, 416–421 (2015).
153. Jariwala, D. et al. Gate-tunable carbon nanotube-MoS_2 heterojunction p-n diode. *Proc. Natl Acad. Sci. USA* **110**, 18076–18080 (2013).
154. Crespo, J. L., Duro, R. J. & Pena, F. L. Gaussian synapse ANNs in multi- and hyperspectral image data analysis. *IEEE Trans. Instr. Meas.* **52**, 724–732 (2003).
155. Sebastian, A., Pannone, A., Subbulakshmi Radhakrishnan, S. & Das, S. Gaussian synapses for probabilistic neural networks. *Nat. Commun.* **10**, 4199 (2019).
156. Zou, X., Liu, M., Shi, Z. & Yakobson, B. I. Environment-controlled dislocation migration and superplasticity in monolayer MoS_2. *Nano Lett.* **15**, 3495–3500 (2015).
157. Onofrio, N., Guzman, D. & Strachan, A. Atomic origin of ultrafast resistance switching in nanoscale electrometallization cells. *Nat. Mater.* **14**, 440–446 (2015).
158. Li, D. et al. MoS_2 memristors exhibiting variable switching characteristics toward biorealistic synaptic emulation. *ACS Nano* **12**, 9240–9252 (2018).
159. Yin, X. et al. Edge nonlinear optics on a MoS_2 atomic monolayer. *Science* **344**, 488–490 (2014).
160. Brooks, R. A. Intelligence without representation. *Art. Intell.* **47**, 139–159 (1991).
161. Strukov, D. B. & Williams, R. S. Four-dimensional address topology for circuits with stacked multilayer crossbar arrays. *Proc. Natl Acad. Sci. USA* **106**, 20155–20158 (2009).
162. Schaibley, J. R. et al. Valleytronics in 2D materials. *Nat. Rev. Mater.* **1**, 16055 (2016).
163. Someya, T., Bao, Z. & Malliaras, G. G. The rise of plastic bioelectronics. *Nature* **540**, 379–385 (2016).
164. O'Reilly, R. C. Biologically based computational models of high-level cognition. *Science* **314**, 91–94 (2006).

Acknowledgements

The work was supported by the National Science Foundation Materials Research Science and Engineering Center at Northwestern University (NSF DMR-1720139).

Competing interests
The authors declare no competing interests.

Additional information
Correspondence should be addressed to M.C.H.

Peer review information *Nature Nanotechnology* thanks Yuchao Yang and the other, anonymous, reviewer(s) for their contribution to the peer review of this work.